Dalton Transactions

ROYAL SOCIETY OF CHEMISTRY

PAPER

View Article Online
View Journal | View Issue

Check for updates

Cite this: *Dalton Trans.*, 2025, **54**, 17932

A hydrogen-bond-stabilized chiral tetrakis Eu(III) complex with strong circularly polarized luminescence

Kun Qian,[a] Blanka Klepetářová,[b] Petr Bouř [b] and Tao Wu *[b]

Received 25th September 2025,
Accepted 3rd November 2025

DOI: 10.1039/d5dt02294k

rsc.li/dalton

We report the synthesis and properties of a hydrogen-bond-stabilized chiral tetrakis Eu(III) complex with enhanced circularly polarized luminescence (CPL). It is based on a Eu(III) tris[3-(heptafluoropropylhydroxymethylene)-camphorate] complex modified with tetrabutylammonium and imidazolium counterions. While the bulky tetrabutylammonium cation preserves the parent tris-diketonate framework, the smaller imidazolium cation forms a novel chiral tetrakis Eu(III) complex through stable NH···O=C hydrogen bonding between the imidazolium N–H donor and the diketonate carbonyl acceptor. A single-crystal X-ray diffraction study indicates a square-antiprismatic geometry. CPL spectra, recorded with a Raman optical activity (ROA) spectrometer under 532 nm excitation, reveal an extremely high dissymmetric factor of 1.26 at 595 nm. In chloroform solution, additional ROA signals were detected, attributed to CPL-induced Raman scattering from the solvent. These properties highlight the convenience of hydrogen-bond-assisted stabilization. The results document an efficient approach for tuning CPL-active lanthanide complexes and demonstrate the methodological advantage of ROA-based CPL detection.

Introduction

Circularly polarized luminescence (CPL) is a convenient tool for studying chirality of the excited state, including coordination complexes and supramolecular systems.[1–3] CPL performance is commonly evaluated using the luminescence dissymmetry factor, $g_{lum} = 2\,(I_L - I_R)/(I_L + I_R)$, where I_L and I_R represent the intensities of left- and right-circularly polarized emission, respectively. However, high values of g_{lum} (close to 2) are extremely rare,[4–6] and achieving them remains a challenge in the design of CPL-active materials.

Furthermore, lanthanide complexes are particularly attractive CPL emitters. They typically provide narrow f–f bands and long lifetimes, and their properties can be tuned using organic ligands.[7–9] A landmark example is the heterobimetallic complex $Cs^+[Eu((+)\text{-hfbc})_4]^-$ (hfbc = 3-heptafluorobutyrylcamphorate), which exhibits a remarkable g_{lum} of 1.38.[4] More recent studies have indicated the decisive role of counterions. For example, replacing Cs^+ with smaller alkylammonium cations further enhanced the CPL response.[10] CH···F interactions with tailored counterions can also stabilize chiral Eu(III) architectures with improved CPL performance due to ligand-to-metal charge transfer (LMCT).

Accurate determination and control of CPL signals remains a methodological challenge.[11] Variations in the excitation wavelength, detection sensitivity, and the sample environment can produce discrepancies in reported g_{lum} values, complicating cross-study comparisons. Methodological advances are therefore needed to ensure both sensitivity and reproducibility in CPL measurements.

Previously, we have demonstrated that a Raman optical activity (ROA) spectrometer can be used for lanthanide CPL studies.[12–15] ROA instruments can normally detect minor differences in vibrational Raman scattering between right- and left-circularly polarized light. When operated under 532 nm excitation, their high laser intensity and artifact-resistant detection enable sensitive monitoring of even weak Eu(III) CPL bands. Because lanthanide complexes exhibit negligible absorption and electronic circular dichroism (ECD) in the visible range,[16,17] interference from these signals is minimal. At 532 nm, the vibrational transitions are usually weak and often dominated by lanthanide CPL. In contrast, near-IR excitation at 785 nm effectively suppresses fluorescence, allowing the determination of vibrational ROA and CPL contributions. For example, vibrational bands of several Eu(III) complexes could be assigned in this case with the aid of density functional theory (DFT) simulations.[12]

Here, we explore a counterion variation in Eu(III) camphorate complexes. It appears that tetrabutylammonium cations preserve the parent tris-Eu(III) framework, whereas imidazolium (ImH) cations form so far undescribed hydrogen-bond-stabilized tetrakis species, $ImH^+[Eu(hfbc)_4]^-$, with a square-antiprismatic geometry

[a]*College of Pharmacy, Jiangxi University of Chinese Medicine, Nanchang, 330004, P. R. China*
[b]*Institute of Organic Chemistry and Biochemistry, Czech Academy of Sciences, Flemingovo náměstí 2, 16 610 Prague, Czech Republic. E-mail: tao.wu@uochb.cas.cz*

determined by single-crystal X-ray diffraction. In contrast, the introduction of sodium hydroxide as a pH balancing agent disrupted this ion pair and yielded a heterobimetallic $Na^+[Eu(hfbc)_4]^-$ complex. The CPL spectrum of $ImH^+[Eu((-)\text{-}hfbc)_4]^-$ recorded with an ROA spectrometer under 532 nm excitation exhibits a high dissymmetry factor (g_{lum} = −1.26 at 595 nm) for the imidazolium-stabilized complex. ROA signals from the solvent affected by Eu(III) CPL were observed in chloroform. This phenomenon is often distinct from ECD-Raman interference,[17] which is negligible in this spectral region.

Experimental

All chemicals were purchased from Sigma Aldrich and used without any further purification.

Synthesis of europium(III) tris[3-(heptafluoropropylhydroxymethylene)-camphorate] Eu(hfc)$_3$

0.53 mmol (225 μl) of (+)-(hfc)$_3$ ((+)-3-(heptafluorobutyryl)-(+)-camphor) or (−)-(hfc)$_3$ ((−)-3-(heptafluorobutyryl)-(−)-camphor) was dissolved in 3 ml of ethanol, then an equivalent molar amount of Et_3N (0.53 mmol, 75 μl) was added slowly upon stirring, and the mixture was kept under stirring for 1 h. Then 0.177 mmol (65 mg) of $EuCl_3{\cdot}6H_2O$ in 2 ml of ethanol was added. After 2 h, ethanol was removed and treated with CH_2Cl_2 : H_2O = 1 : 1, the organic layer was further washed with water and concentrated *in vacuo*. The dried product (262 mg, yielding 12.3%) was used directly in the following steps.

Synthesis of imidazolium tetrakis(3-heptafluoro-butylryl-camphorato) europium(III) $ImH^+[Eu(hfbc)_4]^-$

To a 9 ml ethanol solution of 0.05 mmol (59 mg) of Eu-(+)-(hfc)$_3$ or Eu-(−)-(hfc)$_3$, 0.1 mmol (104.5 mg) of imidazole hydrochloride (ImH) dissolved in 1 ml of ethanol was added slowly under stirring, and the mixture was refluxed for 15 h. A yellow powder was obtained after the solution cooled down and the solvent was removed partially. The crude product was recrystallized in acetonitrile (MeCN) solution, and 9.48 mg of yellow needle crystals were collected, with a yield of 15%. ESI-MS (*m*/*z*): $[Eu(+hfbc)_4]^-$ calcd for $C_{56}H_{56}EuF_{28}O_8$, 1541.27; found, 1541.27. Elemental analysis: calcd for $C_{59}H_{61}EuF_{28}N_2O_8$, C 44.01, H 3.82, N 1.74; found, C 43.79, H 3.66, N 1.88%. $ImH^+[Yb((-)\text{-}hfbc)_4]^-$ was prepared following the same procedure as for the Eu analogue, with Yb^{3+} used instead of Eu^{3+}.

Synthesis of sodium tetrakis(3-heptafluoro-butylryl-camphorato) europium(III) $Na^+[Eu(hfbc)_4]^-$

0.37 mmol (73 mg) of tetraethylammonium iodide or equivalent imidazole hydrochloride and 0.19 mmol (81.4 mg) of Eu$(NO_3)_3{\cdot}5H_2O$ were dissolved in 3 ml of ethanol and added slowly to 3 ml ethanol solution of 0.57 mmol (242 μl) of (+)-(hfc)$_3$ or (−)-(hfc)$_3$. The pH value of the mixture was neutralized to 7 by adding drops of saturated ethanol solution of NaOH. The mixture was stirred for 1 h, and a white precipitate was filtered; a light yellow powder was obtained after the solvent was removed. The crude product was recrystallized in MeCN solution and 76 mg (yield 7%) of light yellow crystals were collected. ESI-MS (*m*/*z*): $[Eu(+hfbc)_4]^-$ calcd for $C_{56}H_{56}EuF_{28}O_8$, 1541.27; found, 1541.27. Elemental analysis: calcd for $C_{58}H_{59}EuF_{28}NO_8$ (based on crystal structure data) C 43.40, H 3.71, N 0.87; found, C 43.22, H 3.45, N 1.02%.

Spectroscopic measurements

The CPL spectra were measured using a ZEBR Raman optical activity (ROA) spectrometer equipped with two CCD cameras, operating in an extended spectral range of 80–4580 cm^{-1} (~534–703 nm) under laser excitation of 532 nm.[18,19] For luminescence bands, the Raman shift/wavenumber (ν_R, in cm^{-1}) can be converted to the absolute wavelength scale (ν_A, in nm) using $\nu_A = 10^7/(10^7/532 - \nu_R)$. The CPL dissymmetry factor g_{lum} value is reported as −2CID, where CID (circular intensity difference) is the ROA analogue of the dissymmetry factor and is expressed as $CID = (I_R - I_L)/(I_R + I_L)$.[13,16] The laser power was 90 mW for $ImH[Eu(hfbc)_4]$ and 30 mW for $Na[Eu(hfbc)_4]$; ROA experiments were carried out with an accumulation time of 5 minutes to capture the intense CPL bands, while longer acquisition times (up to 2 hours) were employed to acquire weaker spectral features with higher resolution.

The ^{1}H NMR spectrum of $ImH^+[Yb(hfbc)_4]^-$ was measured with a Bruker Avance III™ HD 400 MHz spectrometer at ambient temperature in deuterated chloroform.

The ECD spectra were recorded on a Jasco J-815 spectropolarimeter in the range of 350–600 nm. All experiments were performed at room temperature, in a 2 mm quartz cell, and in methanol solutions; the concentration was 2×10^{-3} mol L^{-1} for both complexes.

The fluorescence/luminescence spectra of $ImH^+[Eu(hfbc)_4]^-$ and $Na^+[Eu(hfbc)_4]^-$ complexes in chloroform were recorded on a Fluorolog-QM spectrophotometer (Horiba) equipped with a xenon lamp as the excitation source. Steady-state emission spectra were measured using excitation wavelengths of 360, 370 and 380 nm, respectively. Fluorescence lifetimes at room temperature were measured with the same instrument, using a Spectro LED excitation source (Horiba).

Computations

Equilibrium geometries of $ImH^+[Eu((-)\text{-}hfbc)_4]^-$ and $Na^+[Eu((-)\text{-}hfbc)_4]^-$ were obtained by energy minimization using the Gaussian16 program[20] with the B3LYP functional. For C, H, N, O and F atoms, the 6-311++G(d,p) basis set was employed for the two Eu(III) complexes. The SDF10 and MWB28 pseudopotentials and basis sets were used for Na in $Na^+[Eu((-)\text{-}hfbc)_4]^-$ and for Eu in both complexes, respectively. The conductor-like polarizable continuum solvent model (CPCM) was applied to mimic the environment ($CHCl_3$).[12,21]

Results and discussion

Recent studies have established that both counterion interactions with the tetrakis europium anion and ligand–metal

coupling are critical determinants of CPL performance.[10] In this work, we employed tetrabutylammonium and imidazolium cations to modulate the Eu(III) tris[3-(heptafluoropropylhydroxymethylene)-camphorate] complex. Whereas the bulky tetrabutylammonium cation leaves the parent tris-diketonate framework essentially unaltered, the smaller imidazolium cation promotes the formation of a novel chiral tetrakis Eu(III) species. In contrast, neutralization with sodium hydroxide prevents incorporation of the imidazolium counterion, affording instead the heterobimetallic complex $Na^+[Eu(hfbc)_4]^-$.

Single-crystal X-ray diffraction analyses of $ImH^+[Eu((-)\text{-}hfbc)_4]^-$ (Fig. 1) and $Na^+[Eu((-)\text{-}hfbc)_4]^-$ (Fig. 2) unambiguously confirm these structural motifs, with the key crystallographic parameters summarized in Tables S1 and S2.

The coordination geometry of the Eu core in $ImH^+[Eu((-)\text{-}hfbc)_4]^-$ adopts the typical square antiprism (SAP) arrangement (Fig. 1B), consistent with other reported chiral tetrakis Eu(III) complexes.[4,5,10] Notably, however, this complex crystallizes in the orthorhombic crystal system with the chiral space group $P2_12_12_1$, distinct from the previously reported tetrakis Eu(III) complexes stabilized by small alkylammonium cations.[10] The asymmetric unit comprises four 3-heptafluorobutyrylcamphor $[C_{14}H_{15}F_7O_2]^-$ anions, one Eu^{3+} ion, and one imidazolium $[C_3H_4N_2]^+$ cation, corresponding to the formula $[C_{59}H_{61}EuF_{28}N_2O_8]$ (Fig. 1A). In the eight-coordinated $[EuO_8]$ core, the dihedral angle between the projected planes of adjacent oxygen atoms is −42° (Fig. 1B), similar to the typical square antiprism geometry of its analogue.[5]

The crystal structure reveals a key stabilization feature: a strong N–H···O=C hydrogen bond forms between the N–H group of the imidazolium cation and the carbonyl oxygen atom of the diketonate ligands. The donor–acceptor distance for this interaction is 1.973 Å. Furthermore, an identical hydrogen bond, with a slightly longer distance of 2.055 Å, connects the complex to a second, adjacent $ImH^+[Eu((-)\text{-}hfbc)_4]^-$ molecule (Fig. 1C). Thus, the well-defined hydrogen bonding stabilizing the complexes differs from the ligand-to-ligand hydrogen bonding observed previously.[22,23]

In addition, several weaker C–H···FC interactions were observed between the fluorine substituents of the ligands and the imidazolium cation, with contact distances in the range of 2.672–2.827 Å. These cooperative interactions collectively stabilize the tetrakis Eu(III) framework.

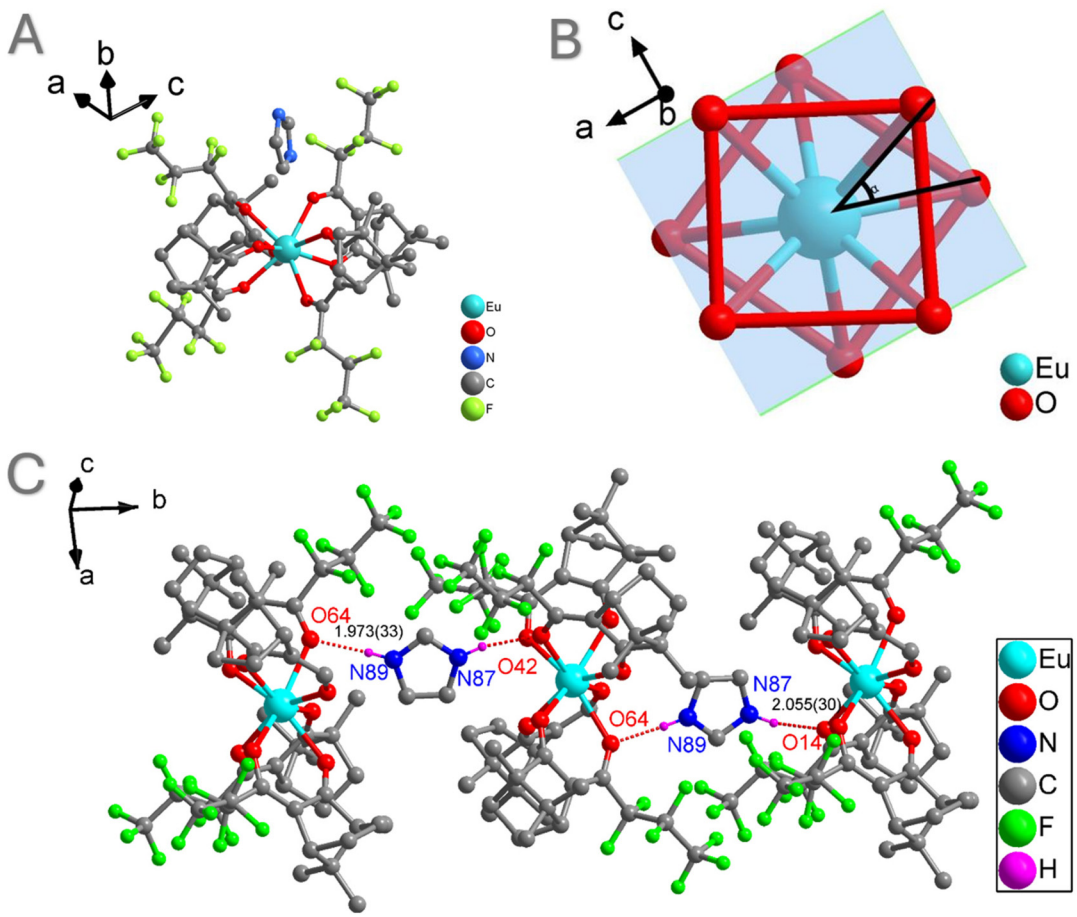

Fig. 1 (A) The asymmetric unit diagram, (B) coordination environment of the Eu^{3+} ion of complex $ImH^+[Eu((-)\text{-}hfbc)_4]^-$, and (C) the presence of CO···HN hydrogen bonds between imidazolium and oxygen atoms of the diketonate ligand.

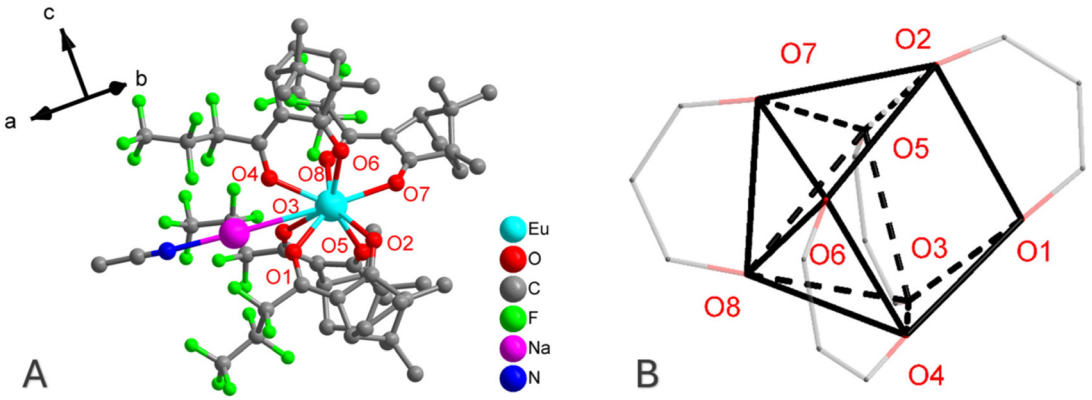

Fig. 2 (A) The asymmetric unit diagram, and (B) DD-8(D2h) configuration of the $Na^+[Eu((-)\text{-hfbc})_4]^-$ complex.

In contrast, the crystal structure of $Na^+[Eu((-)\text{-hfbc})_4]^-$ is closely related to previously described systems exhibiting a "pseudo-achiral DD (D2d)" configuration (Fig. 2B), which also crystallize in the orthorhombic $P2_12_12_1$ space group.[24–26] Here, the Na^+ ion is nine-coordinate, encapsulated by the tetrakis europium anion through multiple $Na^+\cdots$O–Eu and $Na^+\cdots$FC contacts, giving rise to a compact ion pair. Additionally, one nitrogen atom from a solvated CH_3CN molecule binds directly to Na^+ (Fig. 2A).

Paramagnetic NMR of the Yb^{3+} analogue is often used to gain structural insights into Eu^{3+} complexes in solution. Indeed, two broad bands at $\delta > 12$ in the paramagnetic ^{1}H NMR spectrum of $ImH^+[Yb(hfbc)_4]^-$ confirm the presence of the imidazolium cation (Fig. S1). The DFT optimized geometries of both complexes closely reproduce the crystallographic structures (Fig. 3). For $ImH^+[Eu((-)\text{-hfbc})_4]^-$, the calculated distance between the N–H group of the imidazolium cation and the carbonyl oxygen atom of the diketonate ligands of 1.760 Å is slightly shorter than in the crystal. This is consistent with the tendency of DFT to slightly strengthen directional hydrogen bonds in the absence of lattice packing effects. These data highlight the structural flexibility of the $[Eu(hfbc)_4]^-$ framework: in the imidazolium salt, stabilization is dominated by directional N–H$\cdots$O=C hydrogen bonding, while in the sodium salt, it is governed by electrostatic $Na^+\cdots$O/F interactions. Despite these differences, both complexes adopt the Λ-configuration of the camphorate ligands, consistent with previously reported tetrakis Eu(III) architectures.[24,25]

Raman/luminescence ($I_R + I_L$) and ROA/CPL ($I_R - I_L$) spectra of $ImH^+[Eu((\pm)\text{-hfbc})_4]^-$ and $Na^+[Eu((\pm)\text{-hfbc})_4]^-$ enantiomer complexes in chloroform and acetonitrile solutions were measured using an ROA spectrometer equipped with two CCD cameras covering the spectral ranges of 80–2630 cm^{-1} (~534–618 nm) and 2200–4580 cm^{-1} (~603–703 nm). Most luminescence bands of $ImH^+[Eu((-)\text{-hfbc})_4]^-$ and $Na^+[Eu((-)\text{-hfbc})_4]^-$ observed in the Raman scattering closely match those recorded using conventional fluorescence spectroscopy (Fig. S2 and S3). Emission decay curve measurements reveal that the luminescence lifetime of $ImH^+[Eu((-)\text{-hfbc})_4]^-$ is shorter than that of $Na^+[Eu((-)\text{-hfbc})_4]^-$ (Fig. S4), although this difference does not significantly influence the recorded total luminescence or CPL spectra. The CCD detector clearly resolved the characteristic Eu(III) transitions: $^5D_1 \rightarrow {}^7F_2$ (~550–560 nm), $^5D_0 \rightarrow {}^7F_0$ (~580 nm), $^5D_0 \rightarrow {}^7F_1$ (~583–598 nm), $^5D_0 \rightarrow {}^7F_2$ (~610–625 nm), $^5D_0 \rightarrow {}^7F_3$ (~640–660 nm), and $^5D_0 \rightarrow {}^7F_4$ (~690–700 nm).

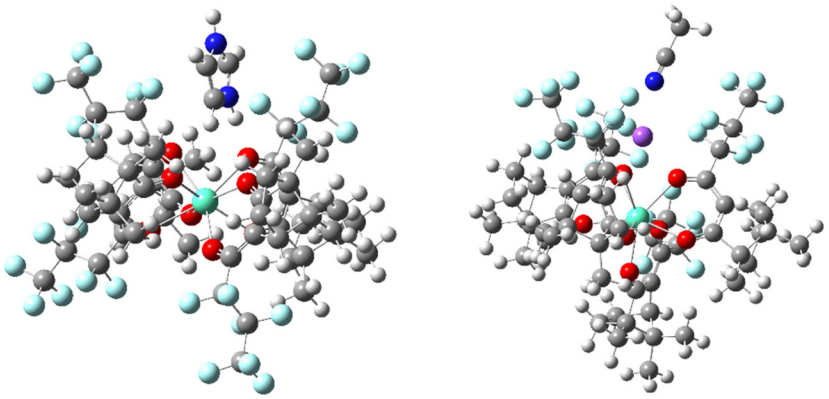

Fig. 3 DFT optimized geometries of complexes $ImH^+[Eu((-)\text{-hfbc})_4]^-$ (left) and $Na^+[Eu((-)\text{-hfbc})_4]^-\cdot CH_3CN$ (right).

The structure of $ImH^+[Eu((\pm)\text{-hfbc})_4]^-$ appears highly stable in both solvents, as the CPL ($I_R - I_L$) patterns of the Eu(III) transitions are almost identical in chloroform (Fig. 4) and acetonitrile (Fig. 5). However, the luminescence dissymmetry factors differ significantly, with chloroform showing a much larger value of 1.26 at the $^5D_0 \rightarrow {}^7F_1$ (595 nm) transition (Table 1). In the low wavenumber range of 100–760 cm^{-1} (530–550 nm), where the Raman signals of chloroform overlap with the chir-

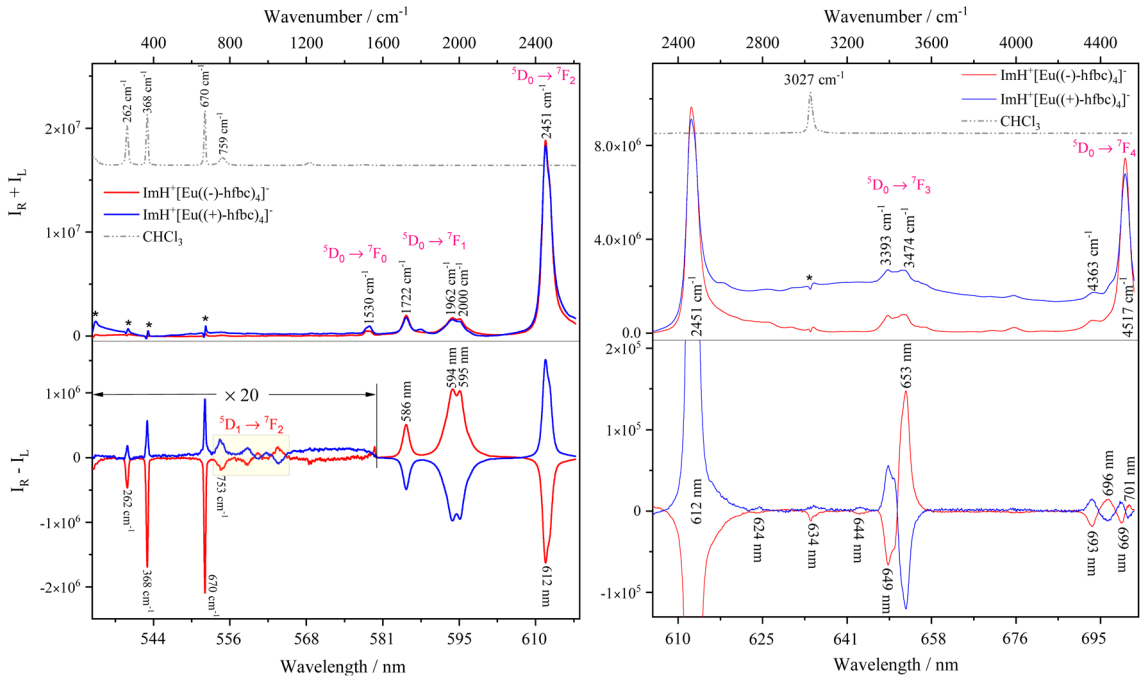

Fig. 4 Raman/luminescence ($I_R + I_L$) and ROA/CPL ($I_R - I_L$) spectra of $ImH^+[Eu((\pm)\text{-hfbc})_4]^-$ enantiomer complexes (3 mM) in chloroform in the range of 80–2630 cm^{-1} (left) and 2280–4580 cm^{-1} (right). Minor artifacts (marked by asterisks [*]) are due to subtracting the chloroform signal.

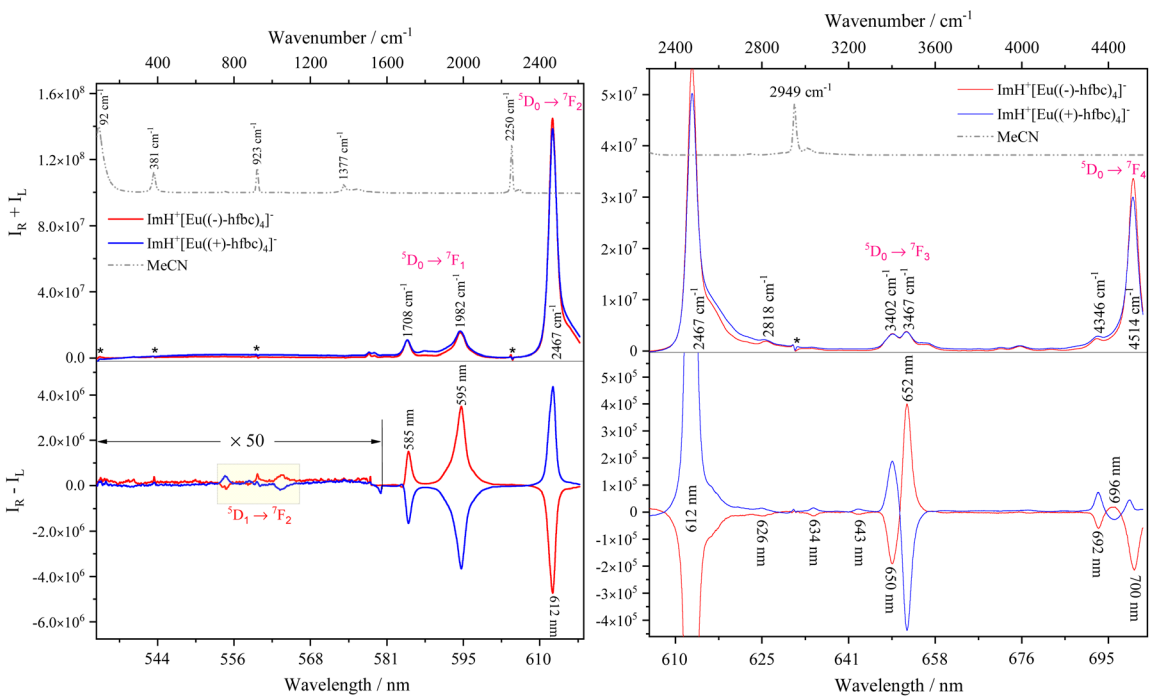

Fig. 5 Raman/luminescence ($I_R + I_L$) and ROA/CPL ($I_R - I_L$) spectra of $ImH^+[Eu((\pm)\text{-hfbc})_4]^-$ enantiomer complexes (1 mM) in acetonitrile in the range of 80–2630 cm^{-1} (left) and 2280–4580 cm^{-1} (right). Minor artifacts (marked by asterisks [*]) are due to subtracting the acetonitrile signal.

Table 1 Circularly polarized luminescence parameters of Eu(III) complexes in chloroform and acetonitrile

Complex	^7F_J	g_{lum} in $CHCl_3$		g_{lum} in MeCN	
$ImH^+[Eu((-)\text{-hfbc})_4]^-$	$J = 1$	−0.52	586 nm	0.34	585 nm
	$J = 1$	−1.26	595 nm	0.47	595 nm
	$J = 2$	0.17	612 nm	−0.07	612 nm
	$J = 3$	0.18	649 nm	0.11	650 nm
	$J = 3$	−0.38	653 nm	−0.21	652 nm
	$J = 4$	0.07	693 nm	0.05	692 nm
	$J = 4$	−0.04	696 nm	−0.01	696 nm
$Na^+[Eu((-)\text{-hfbc})_4]^-$	$J = 1$	−0.12	585 nm	0.05	584 nm
	$J = 1$	−0.13	591 nm	−0.23	585 nm
	$J = 1$	−0.23	595 nm	−0.41	595 nm
	$J = 2$	0.02	611 nm	0.05	612 nm
	$J = 2$	−0.05	626 nm	0.01	625 nm
				0.03	634 nm
	$J = 3$	0.05	651 nm	0.08	650 nm
	$J = 3$	−0.09	655 nm	−0.15	652 nm
				0.02	677 nm
	$J = 4$	−0.02	693 nm	0.04	692 nm
	$J = 4$	0.02	696 nm	−0.02	696 nm

ality sensitive Eu(III) absorption $^5D_1 \leftarrow {}^7F_1$ (~535 nm)[6] and emission $^5D_1 \rightarrow {}^7F_2$ (~550–560 nm), almost mirror image ROA bands of chloroform were detected at 262, 368, 670 and 753 cm^{-1} (Fig. 4 left). Similar features had been previously observed for $Cs^+[Eu((\pm)\text{-hfbc})_4]^-$ in chloroform.[15] At the low concentration used here, the ECD of the Eu(III) $^5D_1 \leftarrow {}^7F_1$ (~535 nm) transition was not observable using a conventional ECD spectrometer (Fig. S5), confirming that ECD-Raman effects can be neglected.[16,17] We therefore attribute the observed ROA signals in chloroform primarily to solvent polarized Raman scattering, coupled with contributions from CPL arising from Eu(III) transitions.

Although the g_{lum} values in acetonitrile are only about half of those in chloroform, no ROA bands assignable to acetonitrile vibrations were detected (Fig. 5). The reduced CPL dissymmetry factor is likely associated with solvent-induced perturbations of the Eu^{3+} excited states. Coupling of the $^5D_0 \rightarrow {}^7F_1$ and $^5D_0 \rightarrow {}^7F_2$ transitions with the C≡N stretching vibrations of acetonitrile (~2250 cm^{-1}) may promote nonradiative relaxation and subtly alter the local electric dipole environment, thereby influencing the observed CPL response.

For $Na^+[Eu((\pm)\text{-hfbc})_4]^-$, both the luminescence ($I_R + I_L$) and CPL ($I_R - I_L$) spectral patterns differ significantly between chloroform (Fig. 6) and acetonitrile (Fig. 7), most likely due to the coordination of one acetonitrile molecule to Na^+ in the solid state. In contrast to the imidazolium system, where larger g_{lum} values are observed in chloroform than in acetonitrile, the sodium analogue shows slightly higher g_{lum} in acetonitrile than in chloroform. The observed CPL bands and g_{lum} values are similar to previous reports obtained with conventional CPL instrumentation.[27] In addition, lower-energy transitions such as $^5D_0 \rightarrow {}^7F_3$ (~640–660 nm) and $^5D_0 \rightarrow {}^7F_4$ (~690–700 nm) were also detected.

Remarkably, a weak but broad band at ~269 cm^{-1} was detected in the acetonitrile solution of $Na^+[Eu((\pm)\text{-hfbc})_4]^-$ (Fig. 7 left) and is attributed to the ECD of the Eu(III) $^5D_1 \leftarrow {}^7F_1$ (~540 nm) transition.[6] A similar pattern was also discernible in the acetonitrile solution of $Na^+[Eu((\pm)\text{-hfbc})_4]^-$ (Fig. 5 left),

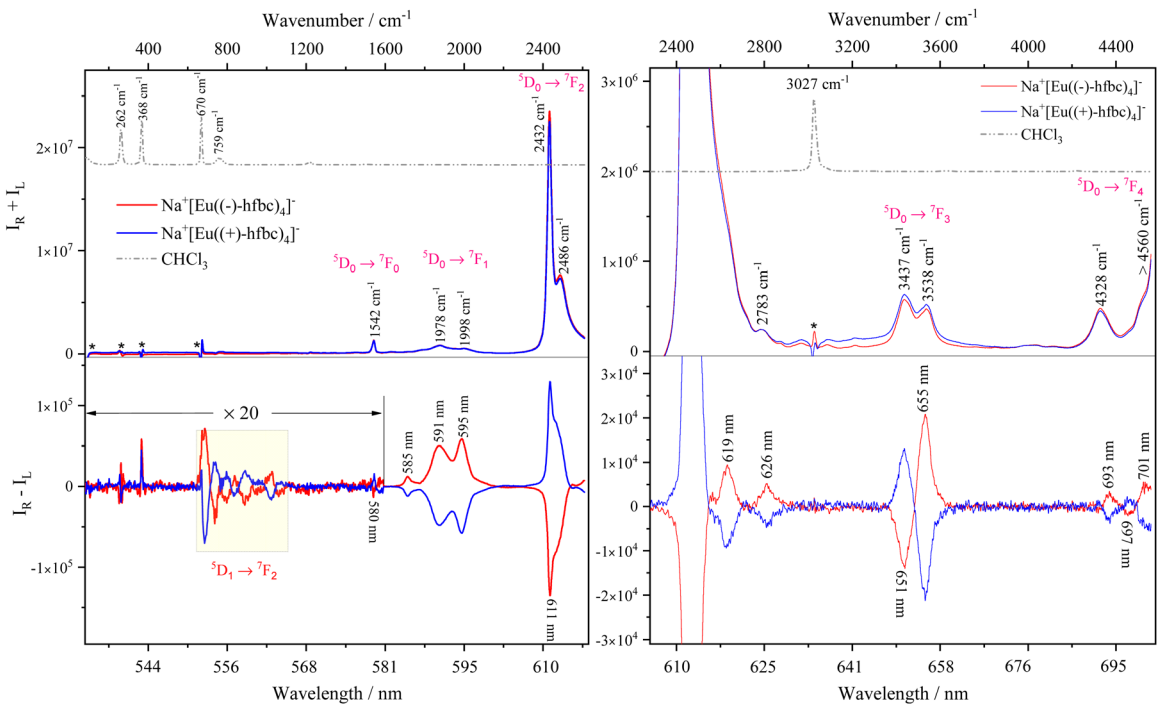

Fig. 6 Raman/luminescence ($I_R + I_L$) and ROA/CPL ($I_R - I_L$) spectra of $Na^+[Eu((\pm)\text{-hfbc})_4]^-$ enantiomer complexes (3 mM) in chloroform in the range of 80–2630 cm^{-1} (left) and 2280–4580 cm^{-1} (right). Minor artifacts (marked by asterisks [*]) are due to subtracting the chloroform signal.

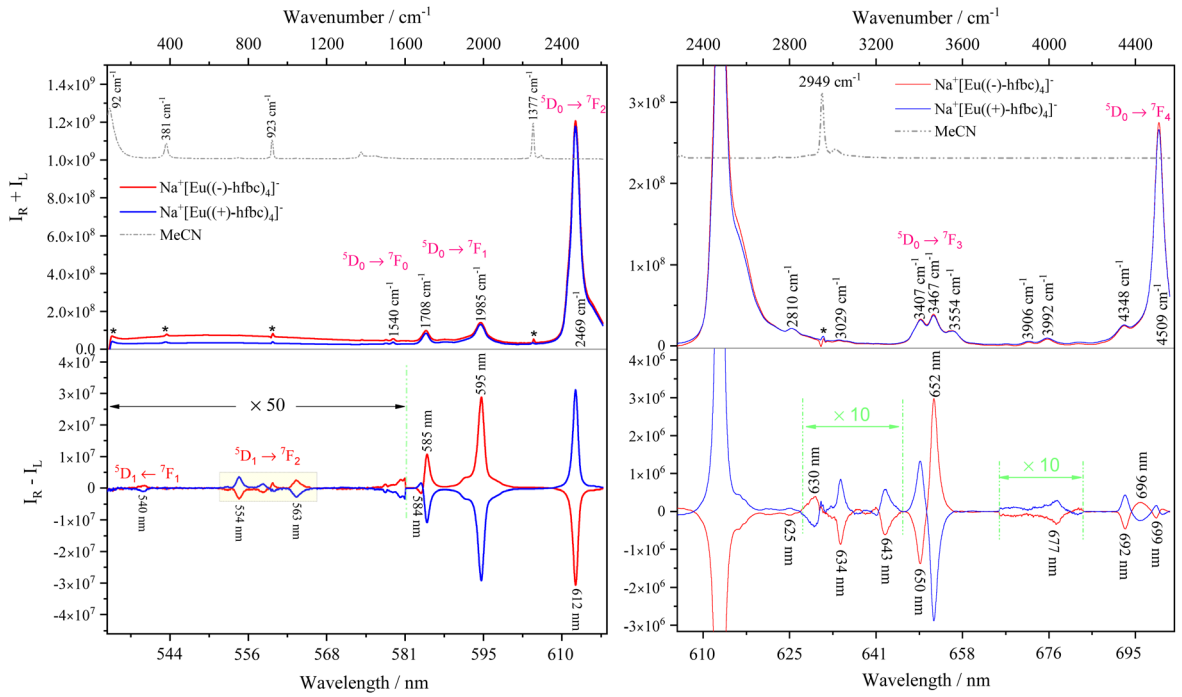

Fig. 7 Raman/luminescence ($I_R + I_L$) and ROA/CPL ($I_R - I_L$) spectra of $Na^+[Eu((\pm)\text{-hfbc})_4]^-$ enantiomer complexes (1 mM) in acetonitrile in the range of 80–2630 cm^{-1} (left) and 2280–4580 cm^{-1} (right). Minor artifacts (marked by asterisks [*]) are due to subtracting the acetonitrile signal.

though somewhat obscured by adjacent solvent noise. Measurement of the degree of circularity[15,17,28] confirmed that these signals do not originate from Raman scattering. Such a feature is extremely difficult to detect in conventional ECD experiments (Fig. S6),[29,30] underscoring the sensitivity of the ROA technique.

Conclusions

In this work, we uncovered a distinct stabilization mechanism in which the imidazolium cation forms strong N–H···O=C hydrogen bonds with the diketonate carbonyl groups, yielding a stable chiral tetrakis Eu(III) complex, $ImH^+[Eu(hfbc)_4]^-$. This architecture represents a different structural motif compared to earlier ammonium-stabilized systems, where steric hindrance prevented hydrogen bonding. Single-crystal X-ray diffraction unambiguously confirms the unique framework.

The $ImH^+[Eu((-)\text{-hfbc})_4]^-$ complex exhibited a large CPL dissymmetry factor of −1.26 at 595 nm, among the highest reported for hydrogen-bond-stabilized Eu(III) complexes and comparable to the benchmark Cs^+ system.[31,32] The emergence of such high CPL activity in a solution-stable ion-pair underscores the crucial role of the imidazolium counterion in modulating the excited-state chiroptical response.

We also find the use of a ROA spectrometer for CPL detection important for the methodology as a toolkit for studying lanthanide optical activity. High-intensity laser excitation enabled the detection of weak Eu(III) bands and allowed separation of CPL from vibrational ROA signals in chloroform solutions. The observation of the Eu(III) ECD transition ($^5D_1 \leftarrow {}^7F_1$) in $Na^+[Eu(hfbc)_4]^-$ further illustrated the sensitivity of ROA to subtle structural and electronic variations.

Overall, the results show that the hydrogen-bond-assisted stabilization is a powerful approach for tuning CPL-active lanthanide complexes and demonstrate the unique potential of ROA-based CPL spectroscopy. Future studies will focus on elucidating the interplay between structure, counterion effects, and solvent-induced Raman interference in lanthanide chiroptical systems.

Author contributions

Experiments: QK, BK, and TW; computation: TW; experimental data analysis: QK, BK, and TW; calculation analysis: PB and TW; writing of the manuscript: QK and TW; review and editing: all authors; funding acquisition: QK and TW.

Conflicts of interest

There are no conflicts to declare.

Data availability

The data supporting this article have been included as part of the supplementary information (SI). Supplementary information: crystallographic data, ^1H NMR spectrum of Yb

complex, emission spectra with the corresponding emission decay profiles and ECD spectra of the complexes. See DOI: https://doi.org/10.1039/d5dt02294k.

CCDC 2450564 and 2450565 contain the supplementary crystallographic data for this paper.[33a,b]

Acknowledgements

This work was supported by the Czech Science Foundation (23-05378S) and the National Natural Science Foundation of China (22165014).

References

1 X. Yang, X. Gao, Y.-X. Zheng, H. Kuang, C.-F. Chen, M. Liu, P. Duan and Z. Tang, Recent Progress of Circularly Polarized Luminescence Materials from Chinese Perspectives, *CCS Chem.*, 2023, **5**, 2760–2789.
2 L. Arrico, L. Di Bari and F. Zinna, Quantifying the Overall Efficiency of Circularly Polarized Emitters, *Chem. – Eur. J.*, 2021, **27**, 2920–2934.
3 T. Zhao, J. Han, P. Duan and M. Liu, New Perspectives to Trigger and Modulate Circularly Polarized Luminescence of Complex and Aggregated Systems: Energy Transfer, Photon Upconversion, Charge Transfer, and Organic Radical, *Acc. Chem. Res.*, 2020, **53**, 1279–1292.
4 J. L. Lunkley, D. Shirotani, K. Yamanari, S. Kaizaki and G. Muller, Extraordinary circularly polarized luminescence activity exhibited by cesium tetrakis(3-heptafluoro-butylryl-(+)-camphorato) Eu(III) complexes in EtOH and CHCl3 solutions, *J. Am. Chem. Soc.*, 2008, **130**, 13814–13815.
5 S. Di Pietro and L. Di Bari, The Structure of MLn(hfbc)(4) and a Key to High Circularly Polarized Luminescence, *Inorg. Chem.*, 2012, **51**, 12007–12014.
6 F. S. Richardson, Selection-Rules for Lanthanide Optical-Activity, *Inorg. Chem.*, 1980, **19**, 2806–2812.
7 G. Muller, Luminescent chiral lanthanide(III) complexes as potential molecular probes, *Dalton Trans.*, 2009, **38**, 9692–9707.
8 R. Carr, N. H. Evans and D. Parker, Lanthanide complexes as chiral probes exploiting circularly polarized luminescence, *Chem. Soc. Rev.*, 2012, **41**, 7673–7686.
9 F. Zinna and L. Di Bari, Lanthanide Circularly Polarized Luminescence: Bases and Applications, *Chirality*, 2015, **27**, 1–13.
10 M. Tsurui, R. Takizawa, Y. Kitagawa, M. Wang, M. Kobayashi, T. Taketsugu and Y. Hasegawa, Chiral Tetrakis Eu(III) Complexes with Ammonium Cations for Improved Circularly Polarized Luminescence, *Angew. Chem., Int. Ed.*, 2024, **63**, e202405584.
11 H. Lu, L. Di Bari and L. Favereau, Standardizing the characterization of circularly polarized luminescence of chiral materials, *Nat. Photonics*, 2025, **19**, 1041–1047.
12 T. Wu, P. Bouř, T. Fujisawa and M. Unno, Molecular Vibrations in Chiral Europium Complexes Revealed by Near-Infrared Raman Optical Activity, *Adv. Sci.*, 2024, **11**, 2305521.
13 T. Wu, A Raman optical activity spectrometer can sensitively detect lanthanide circularly polarized luminescence, *Phys. Chem. Chem. Phys.*, 2022, **24**, 15672–15686.
14 T. Wu, J. Kapitán, V. Andrushchenko and P. Bouř, Identification of Lanthanide(III) Luminophores in Magnetic Circularly Polarized Luminescence Using Raman Optical Activity Instrumentation, *Anal. Chem.*, 2017, **89**, 5043–5049.
15 T. Wu, J. Kapitán, V. Mašek and P. Bouř, Detection of Circularly Polarized Luminescence of a Cs-Eu-III Complex in Raman Optical Activity Experiments, *Angew. Chem., Int. Ed.*, 2015, **54**, 14933–14936.
16 T. Wu, R. Pelc and P. Bouř, Molecular Properties of 3d and 4f Coordination Compounds Deciphered by Raman Optical Activity Spectroscopy, *ChemPlusChem*, 2023, **88**, e202300385.
17 T. Wu, G. Li, J. Kapitán, J. Kessler, Y. Xu and P. Bouř, Two Spectroscopies in One: Interference of Circular Dichroism and Raman Optical Activity, *Angew. Chem., Int. Ed.*, 2020, **59**, 21895–21898.
18 P. Michal, J. Hudecová, R. Čelechovský, M. Vůjtek, M. Dudka and J. Kapitán, Accurate Determination of Enantiomeric Excess Using Raman Optical Activity, *Symmetry*, 2022, **14**, 990.
19 P. Michal, R. Čelechovský, M. Dudka, J. Kapitán, M. Vůjtek, M. Berešová, J. Šebestík, K. Thangavel and P. Bouř, Vibrational Optical Activity of Intermolecular, Overtone, and Combination Bands: 2-Chloropropionitrile and α-Pinene, *J. Phys. Chem. B*, 2019, **123**, 2147–2156.
20 M. J. Frisch, G. W. Trucks, H. B. Schlegel, G. E. Scuseria, M. A. Robb, J. R. Cheeseman, G. Scalmani, V. Barone, G. A. Petersson, H. Nakatsuji, X. Li, M. Caricato, A. V. Marenich, J. Bloino, B. G. Janesko, R. Gomperts, B. Mennucci, H. P. Hratchian, J. V. Ortiz, A. F. Izmaylov, J. L. Sonnenberg, D. Williams-Young, F. Ding, F. Lipparini, F. Egidi, J. Goings, B. Peng, A. Petrone, T. Henderson, D. Ranasinghe, V. G. Zakrzewski, J. Gao, N. Rega, G. Zheng, W. Liang, M. Hada, M. Ehara, K. Toyota, R. Fukuda, J. Hasegawa, M. Ishida, T. Nakajima, Y. Honda, O. Kitao, H. Nakai, T. Vreven, K. Throssell, J. A. Montgomery Jr., J. E. Peralta, F. Ogliaro, M. J. Bearpark, J. J. Heyd, E. N. Brothers, K. N. Kudin, V. N. Staroverov, T. A. Keith, R. Kobayashi, J. Normand, K. Raghavachari, A. P. Rendell, J. C. Burant, S. S. Iyengar, J. Tomasi, M. Cossi, J. M. Millam, M. Klene, C. Adamo, R. Cammi, J. W. Ochterski, R. L. Martin, K. Morokuma, O. Farkas, J. B. Foresman and D. J. Fox, *Gaussian 16*, Revision C.01, 2016.
21 A. Klamt, Conductor-like Screening Model for Real Solvents: A New Approach to the Quantitative Calculation of Solvation Phenomena, *J. Phys. Chem.*, 1995, **99**, 2224–2235.
22 T. Harada, Y. Nakano, M. Fujiki, M. Naito, T. Kawai and Y. Hasegawa, Circularly Polarized Luminescence of Eu(III) Complexes with Point- and Axis-Chiral Ligands Dependent

on Coordination Structures, *Inorg. Chem.*, 2009, **48**, 11242–11250.

23 T. Harada, H. Tsumatori, K. Nishiyama, J. Yuasa, Y. Hasegawa and T. Kawai, Nona-Coordinated Chiral Eu(III) Complexes with Stereoselective Ligand–Ligand Noncovalent Interactions for Enhanced Circularly Polarized Luminescence, *Inorg. Chem.*, 2012, **51**, 6476–6485.

24 Y. J. Lin, F. Zou, S. G. Wan, J. Ouyang, L. R. Lin and H. Zhang, Dynamic chiral-at-metal stability of tetrakis (d/l-hfc)Ln(III) complexes capped with an alkali metal cation in solution, *Dalton Trans.*, 2012, **41**, 6696–6706.

25 D. Shirotani, T. Suzuki, K. Yamanari and S. Kaizaki, Crystal structure and chiroptical spectra of sodium tetrakis (+)-hfbc Pr(III) complex, *J. Alloys Compd.*, 2008, **451**, 325–328.

26 D. Shirotani, T. Suzuki and S. Kaizaki, Novel configurational structures of sodium tetrakis(3-heptafluorobutylryl-(+)-camphorato) Ln(III) complexes with a trapped Na+ by Na+ center dot center dot center dot FC interactions in the solid state and in solution, *Inorg. Chem.*, 2006, **45**, 6111–6113.

27 J. L. Lunkley, D. Shirotani, K. Yamanari, S. Kaizaki and G. Muller, Chiroptical Spectra of a Series of Tetrakis((+)-3-heptafluorobutylyrylcamphorato)lanthanide(III) with an Encapsulated Alkali Metal Ion: Circularly Polarized Luminescence and Absolute Chiral Structures for the Eu(III) and Sm(III) Complexes, *Inorg. Chem.*, 2011, **50**, 12724–12732.

28 W. Hug and G. Hangartner, A novel high-throughput Raman spectrometer for polarization difference measurements, *J. Raman Spectrosc.*, 1999, **30**, 841–852.

29 D. Shirotani, K. Yamanari, R. Kuroda, T. Harada, J. L. Lunkley, G. Muller, H. Sato and S. Kaizaki, Chiroptical Spectra of Tetrakis (+)-3-Heptafluorobutylrylcamphorate Ln (III) Complexes with an Encapsulated Alkali Metal Ion: Solution Structures as Revealed by Chiroptical Spectra, *Chirality*, 2012, **24**, 1055–1062.

30 D. Shirotani, H. Sato, K. Yamanari and S. Kaizaki, Electronic circular dichroism in the 4f–4f transitions of a series of cesium tetrakis (+)-3-heptafluorobutyrylcamphorate Ln(III) complexes, *Dalton Trans.*, 2012, **41**, 10557–10567.

31 L. Llanos, P. Cancino, P. Mella, P. Fuentealba and D. Aravena, Circularly polarized luminescence and coordination geometries in mononuclear lanthanide(III) complexes, *Coord. Chem. Rev.*, 2024, **505**, 215675.

32 D. Thakur and S. Vaidyanathan, Chiral lanthanide complexes in the history of circularly polarized luminescence: a brief summary, *J. Mater. Chem. C*, 2025, **13**, 9410–9452.

33 (*a*) CCDC 2450564: Experimental Crystal Structure Determination, 2025, DOI: 10.5517/ccdc.csd.cc2n80gf; (*b*) CCDC 2450565: Experimental Crystal Structure Determination, 2025, DOI: 10.5517/ccdc.csd.cc2n80hg.